ACOUSTICS 2012

Nonlinear effects in infrasound propagation simulations

O. Gainville[a] and O. Marsden[b]

[a]CEA, DAM, DIF, F-91297 Arpajon, France
[b]Laboratoire de Mecanique des Fluides et d'Acoustique, 36 Av Guy de Collongue 69134 Ecully Cedex
olaf.gainville@cea.fr

In the framework of the Comprehensive Nuclear-Test-Ban Treaty, long range propagation of infrasound through the atmosphere is investigated using numerical models. The study problem is a cylindrical blast in an inhomogeneous atmosphere. Vertical profiles of temperature, wind and density obtained during the Misty Picture High explosive experiment conducted in May 1987 are used. The propagation is simulated using two codes. First, the full 2-D Navier-Stokes equations are solved with a low-dispersion and low-dissipation finite-difference algorithm initially developed for aeroacoustics. Second, a nonlinear ray tracing model based on weak shock and locally plane wave assumptions is used. In this code, the waveform evolves along rays following Burgers' equation. The initialisation of the cylindrical blast wave is described for both codes. A benchmark case of propagation is defined and numerical comparisons are performed. Absorption and nonlinear effects are investigated for both stratospheric and thermospheric paths. Some limits of the ray tracing model are shown and quantified.

1 Introduction

Infrasonic research is highly motivated by the Comprehensive Nuclear-Test-Ban Treaty. The International Monitoring System is developing a network comprising of sixty barometric stations which should be able to detect a one kiloton yield explosion anywhere on the globe. Explosion studies are necessary to evaluate the detection capability of this network and to develop tools for infrasound record analysis. In this context, we develop numerical tools to model the long range propagation of infrasound.

Long range propagation of infrasound is governed at first order by sound speed and wind variations which define tropospheric, stratospheric and thermospheric wave guides. The waveform evolution depends on nonlinear effects and on atmospheric absorption. For explosions, nonlinear effects are dominant during the first stage of the propagation, where shock waves are strong. A 2-D benchmark propagation problem to study nonlinear and classical absorption phenomena in the context of long range atmospheric propagation appears important for the validation and comparison of different codes.

In this article, we define a 2-D propagation benchmark problem with atmospheric data and an initial linear energy source. We present the Navier-Stokes equations solver with a finite-difference algorithm and the weakly nonlinear ray tracing method. Shock waves generated by the source are analysed at short range.

2 2-D propagation problem

The propagation benchmark is designed to study nonlinear and classical absorption phenomenon associated to acoustic wave propagation at long range in the atmosphere. Accordingly, the propagation problem is defined as the resolution of Navier-Stokes equations. The ground is an adiabatic rigid and flat surface. The atmospheric model and the source model are defined below.

2.1 Simple atmospheric model

To define a simple 2-D benchmark propagation reference case, we assume that the air is a perfect gas with a constant specific ratio $\gamma = 1.4$ and a constant molecular weight $M_0 = 28.85\text{e-}3\,\text{kg/mol}$. Atmospheric sound speed c_0 and zonal u_0 wind are functions of altitude z, defined by cubic spline interpolation (see appendix 5.2 and fig. 1). Atmospheric temperature is computed from sound speed: $T_0 = M_0 c_0^2/\gamma R$, with R the perfect gas constant. Hydrostatic equilibrium is used to compute the atmospheric pressure p_0

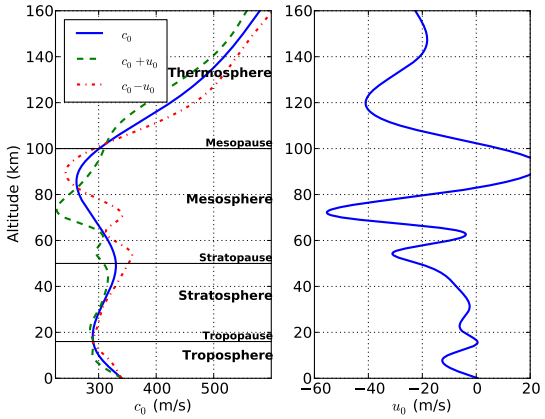

Figure 1: Atmospheric sound speed and zonal wind profiles (see appendix 5.2).

and atmospheric density ρ_0:

$$\frac{\partial p_0}{\partial z} = -\rho_0 g = -\frac{M_0 p_0}{R T_0} g,$$

assuming that gravity g is constant at $9.81\,\text{m/s}^2$. This equation is numerically integrated from the ground $z = 0$ with ground pressure p_g of 101325 Pa.

Viscosity is given by Sutherland's law:

$$\mu(T) = \mu_S \left(\frac{T}{T_S}\right)^{1/2} \frac{1 + S_S/T_S}{1 + S_S/T},$$

with $S_S = 117\,\text{K}$, $\mu_S = 1.18192\text{e-}5\,\text{Pa/s}$ and $T_S = 293.15\,\text{K}$. Bulk viscosity is defined as $\mu_b = 0.6\mu$ and the thermal conductivity coefficient is $\kappa = \mu c_p/P_r$ with a constant Prandlt number $P_r = 3/4$.

Sound speed and wind profiles of fig. 1 are defined to verify both static and dynamic atmospheric stabilities. Static stability is obtained if the Brunt-Väisälä frequency N is always defined (*i.e.* $N^2 > 0$) and dynamic stability is obtained for a Richardson number Ri above approximately 1.

$$N^2 = -\frac{g}{\rho_0}\frac{\partial \rho_0}{\partial z} - \frac{g^2}{c_0^2} = \frac{\gamma g}{c_0^2}\left(\frac{\partial c_0^2/\gamma}{\partial z} + \frac{\gamma - 1}{\gamma} g\right), \quad (1)$$

$$R_i = \frac{N^2}{\left|\frac{\partial u_0}{\partial z}\right|^2}. \quad (2)$$

Profiles of N and Ri as represented at fig. 1. Both stability criteria are well satisfied. These atmospheric profiles are smoothed versions of the Misty Picture atmospheric profiles [6]. Observation of sound speed and wind profiles

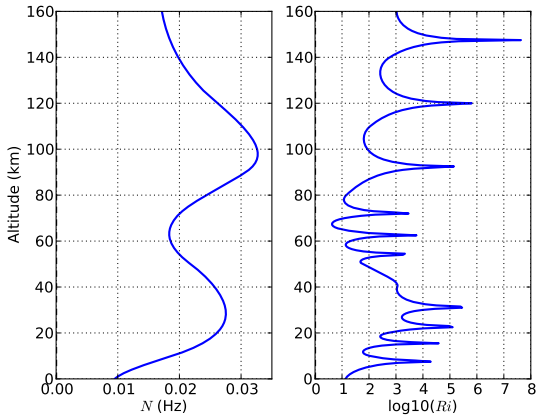

Figure 2: Brunt-Väisälä frequency N and Richardson number Ri of the atmospheric model.

(fig. 1) shows that a stratospheric wave guide is defined toward the West whereas only thermospheric wave guide exists for propagation toward East or without wind.

2.2 Source model

The idealised source is designed to be easily initialised in the finite difference methods and to mimic a point blast behaviour. The source centre is located on the ground. In two dimensions, the equivalent linear source energy is noted E_1 (J/m). The source is an initial Gaussian overpressure distribution [4]:

$$p(x,z,t=0) - p_0(x,z) = Ae^{-\ln 2 \frac{x^2+z^2}{B^2}}, \qquad (3)$$

with B Gaussian half-width and A amplitude of the source defined by:

$$A = (\gamma - 1)E_1 \frac{\ln 2}{\pi B^2}.$$

As the source is located on the ground, the total energy E_1 is twice the spatial integral of internal energy. Density and velocity in the source area remain unchanged, with atmospheric values.

In our numerical application, the Gaussian half width is set to 300 m and the linear source energy at 183 GJ/m (*i.e.* $\approx$ 44 t_{TNT}/m and $A = 1.8e^5$ Pa). This energy has been chosen to give a maximum overpressure of approximately 3000 Pa at 10 km.

3 Numerical acoustics propagation models

In this section are presented the two models used to simulate the propagation of acoustic waves including nonlinear effects and absorption. The first model is a direct numerical resolution of Navier-Stokes equations using finite difference numerical scheme. The second is a ray tracing method with the resolution of the Burgers' equation.

3.1 Finite difference method

The full 2-D Navier-Stokes equations are solved on a regular Cartesian grid with an optimised high-fidelity numerical procedure based on explicit spatial finite differences and Runge-Kutta time integration [12, 7].

Away from boundaries, spatial discretization is performed with explicit fourth-order eleven-point centred finite differences optimised to minimise dispersion for wavenumbers discretized by between 4 and 32 grid points [2]. Close to boundaries, be they solid walls or radiation conditions, optimised explicit non-centred differencing schemes are used [1]. The non-centered differencing schemes are all based on eleven-point stencils, including the one-sided stencil used for wall points. Time integration is performed with a six-step second-order optimised low-storage Runge-Kutta algorithm [2]. Characteristics regarding dispersion and dissipation for the spatial differencing schemes, filters, and the time integration scheme can be found in previous papers [2, 1]. This solver has been validated on reference viscous flow configurations and on a demanding multi-body acoustic scattering test-case, yielding results in good agreement with experimental and analytical data [10, 11].

The schemes' properties mean that the behaviour of waves discretized by at least four points per wavelength is accurately reproduced, with very low levels of dispersion and dissipation, for frequencies such that $\omega\Delta t \leq 1.25 \times \pi$. The determination of the computational time step is based on a CFL criterion, CFL= $c_{max}\Delta t/\Delta x = 0.75$, where c_{max} is the largest value of the speed of sound in the atmosphere modelled here.

Spatial filtering is carried out to ensure stable computations. An explicit 11-point filtering stencil is designed to remove fluctuations discretized by less than four grid points per wavelength, while leaving all larger wavelengths effectively untouched [2]. As the differencing schemes used near boundaries are asymmetric, their effective wavenumbers have an imaginary part which leads to them being unstable for very high frequencies. It is therefore essential to use them in conjunction with appropriate highly selective filters, and to this end, we use the filters described in Berland *et al* [1], which also selectively damp fluctuations with fewer than four points per wavelength. Filters for grid points more than two points away from a boundary are built on eleven-point stencils, while the last and last but one point stencils up to two points away from a boundary are built respectively on four and seven points. Thus at the wall, in the x direction, the centred eleven-point filter is used, whereas in the y direction the family of non-centred filters is applied. At the lateral radiation boundaries in the x and y directions, Tam and Dong's 2-D far-field radiation condition [14] is used.

In addition a non-linear shock-capturing filtering [3] is employed to avoid potential problems for standard finite-differences time-domain acoustic solvers, which are not designed to cope with steep wave fronts and which can lead to Gibbs oscillations.

3.2 Ray tracing code

The ray tracing method models the propagation of acoustic waves in the geometrical acoustic limits and in the weak shock approximation. For a detailed presentation of the ray tracing code and its validation, we refer the reader to Gainville & al. [5, 6].

The ray tracing code solves ray tracing equations and

geodesic elements equations to compute ray trajectory and signature amplitude at first order. Pressure signatures evolve along rays following a generalized Burgers' equation which takes into account nonlinear effects and classical absorption. The pressure signature $p' = p - p_0$ is normalised using the wave action conservation law as:

$$u(\xi, t) = \left(\frac{\nu}{k\rho_0 c_0^3}\right)^{1/2} p'\left(\mathbf{x}(t) + \xi\mathbf{n}/k, t\right), \qquad (4)$$

where ξ is a scaled distance, t is the time curvilinear abscissa along the ray and ν is the convected volume [5] which is proportional to the classical ray tube section [13]. $\mathbf{x}(t)$ is the trajectory of the wavefront and $\mathbf{k} = k\mathbf{n}$ the local wave vector. The Burgers' equation is solved using a Fourier Galerkin spectral scheme:

$$\frac{\partial\tilde{u}(q,t)}{\partial t} = -\Gamma(kq,t)\tilde{u} - \imath\frac{1+\gamma}{2}\left(\frac{c_0 k}{\rho_0\nu}\right)^{1/2}\frac{kq}{2}\widetilde{(u^2)}, \qquad (5)$$

where kq is the acoustic wavelength. $\tilde{u}$ and $\tilde{u^2}$ are respectively Fourier transforms of u and u^2. The linear attenuation coefficient is:

$$\Gamma(kq,t) = \frac{\mu}{2\rho_0}\left(\frac{4}{3} + \frac{\mu_b}{\mu} + \frac{\gamma-1}{P_r}\right)k^2q^2. \qquad (6)$$

Variables depend on the underlying atmospheric state at the position $\mathbf{x}(t)$. Additional specific developments are performed to pass through caustics [5].

Rays are emitted from the source where the wavefront is assumed to be spherical. The waveform signature is initialised at a distance r_{ref} where the shock is assumed weak. This distance should be larger than approximately $2(E_1/p_0)^{1/2}$ [8]. As a first stage of the comparison between codes, the ray tracing model is initialised using a waveform given by the finite difference code. This waveform is taken on the ground at the distance r_{ref} from the source. The connection between codes is performed for variables p'/p_0 as a function of time t. To take into account atmospheric stratification effects, the waveform amplitude is scaled using empirical law of equation (7). In this law, the atmospheric pressure at the observed point should be used. This approximation is discussed in the following section and in [8, 9].

3.3 Shock and acoustic waves at short range

The initial overpressure distribution source produces shock waves which propagate at long range in the atmosphere. In this section, we analyse generated shock waves and effects of the atmospheric pressure exponential decay at short range. We analyse a finite differences simulation performed with an isothermal stratified atmosphere and the source defined above. With a linear source energy of 183 GJ/m, the source characteristic radius is $r_0 = 1345$ m, using atmospheric pressure at the source p_{0s}. We additionally define a local characteristic radius $r_{0l} = (E_1/p_0)^{1/2}$, with p_0 the atmospheric pressure at the point of interest. Then, for the isothermal stratified atmosphere, r_{0l} evolves from r_0 at ground level to 3000 m at 15000 m ($10r_0$) height.

The Gaussian overpressure distribution source generates well formed shock waves (fig. 3). These signatures have

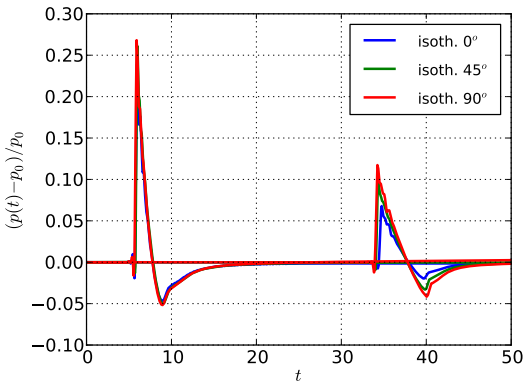

Figure 3: Scaled waveform signature as function of time (s) at distances $2r_0$ and $10r_0$ for three elevations.

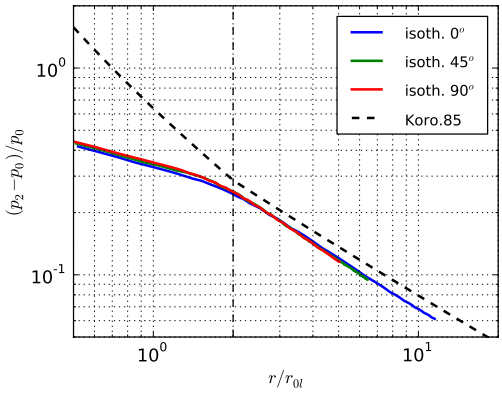

Figure 4: Scaled maximum overpressure as a function of the scaled distance r/r_{0l} for three elevations. The local source characteristic distance is used: $r_{0l} = (E_1/p_0)^{1/2}$, with p_0 at point of interest. Empirical law of Korobeinikov [8] is indicated.

the usual shape of explosion shock waves. In figure 3, signatures are drawn for three elevations (horizontal, 45° and vertical) and at two distances ($2r_0$ and $10r_0$). Influence of the atmospheric pressure on the signature shape is very small.

In figure 4, the scaled maximum overpressure $(p_2 - p_0)/p_0$ obtained by simulations is plotted, for three elevations. The distance is scaled with the local characteristic radius r_{0l}. This scaled distance r/r_{0l} is well adapted since the three curves are very close to each other. Comparison to the homogeneous empirical law (7) is also performed. For $r < 2r_{0l}$, the shock wave has not yet been formed and the simulation does not agree with empirical law. For $r > 2r_{0l}$, the dump of simulated maximum overpressure and of the empirical law is the same, but a shift by a factor 1.1 exits. It is due to smoothing of the signature by the numerical method and to the spatial source distribution. Note that the shock becomes weak for approximately $r > 2r_{0l}$.

The positive phase duration (see figure 5) and the arrival time of the shock t_0 (see figure 6) increase with the scaling distance r/r_0. Their evolution are slightly dependant of the atmospheric pressure.

To conclude this analysis, we note that the initialisation of

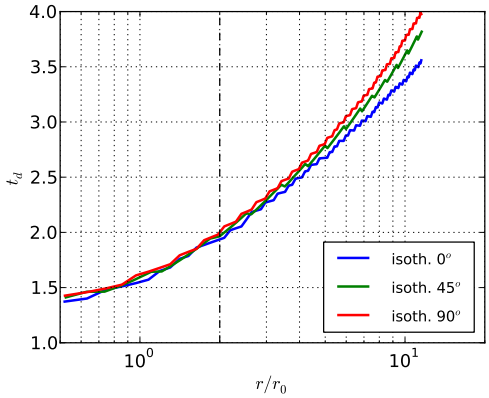

Figure 5: Positive phase duration as a function of the scaled distance r/r_0 for three elevations. Source characteristic distance $r_0 = (E_1/p_{0s})^{1/2}$ with p_{0s} at source position.

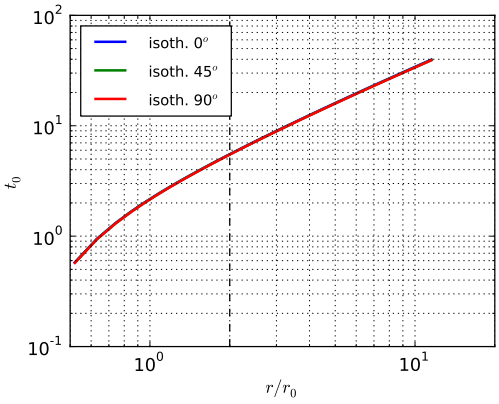

Figure 6: Arrival shock time as a function of the scaled distance r/r_0 for three elevations.

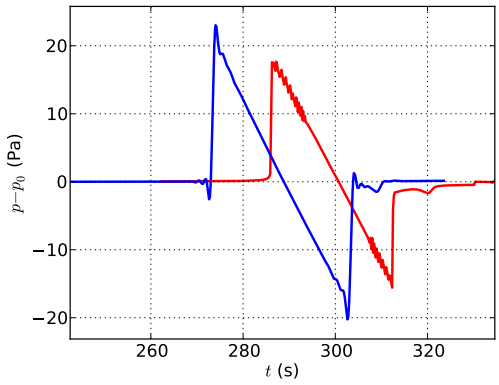

Figure 7: Waveform signature for the ray tracing code (red) and the finite-difference code (blue) at 76.5 km.

the signature in the ray tracing method at a distance $r_{\text{ref}} = 2r_0$ is consistent with both the weak shock approximation and the formation distance of the shock from the initial Gaussian distribution.

3.4 Codes comparison: first results

The waveform signature evolves during propagation because of nonlinear and absorption effects. Waveform signatures obtained at 76.5 km with both codes are presented at figure 7. The same N-wave shape is observed and both amplitude and duration appear similar.

4 Conclusion

In this article, a 2-D long range propagation benchmark is defined. It allows the comparison and validation of codes for wave guide atmospheric effects, nonlinear effects and classical absorption effects. This case is relatively simple with smooth and stable sound speed and wind vertical profiles. The comparison of finite-difference resolution of Navier-Stokes equation with the weakly nonlinear ray tracing code shows good agreement.

5 Appendix

5.1 2-D Point blast empirical law

Point blast problem analysed in homogeneous media have empirical solutions [8] for the maximum shock pressure p_2:

$$\frac{p_2 - p_0}{p_0} = \begin{cases} \frac{4\gamma}{\gamma+1}\left((1+16\gamma\alpha_b Z^2)^{1/2}-1\right)^{-1}, & 0 \le Z \le 2 \\ \frac{4\gamma}{\gamma+1}\left((1+16\sqrt{2}\gamma\alpha_b Z^{3/2})^{1/2}-1\right)^{-1}, & 2 \le Z \end{cases} \tag{7}$$

with $Z = r(E_1/p_0)^{-1/2}$ and $\alpha_b = 0.92$ for $\gamma = 1$ [8].

5.2 Simple atmospheric model data

Sound speed and zonal wind profiles are defined by cubic spline interpolation of table 1 data. Second derivatives of the table are obtained by natural cubic spline interpolation of values. Cubic spline interpolation is defined as follow: for $z \in [z_i, z_{i+1}]$, with $b = \frac{z-z_i}{z_{i+1}-z_i}$ and $a = 1-b$:

$$v = av_i + bv_{i+1} + \frac{1}{6}\left((a^3-a)v_i'' + (b^3-b)v_{i+1}''\right)(z_{i+1}-z_i)^2.$$

References

[1] Berland, J., Bogey, C., Marsden, O., and Bailly, C. High-order, low dispersive and low dissipative explicit schemes for multiple-scale and boundary problems. *Journal of Computational Physics 224*, 2 (2007), 637 – 662.

[2] Bogey, C., and Bailly, C. A family of low dispersive and low dissipative explicit schemes for noise computation,. *J. Comp. Phys. 194*, 1 (2004), 194–214.

z km	c_0 m/s	c_0'' (m/s)/km^2
0	340.	0.
10	300.	0.393119
20	290.	0.227525
50	330.	-0.271106
70	290.	0.0142438
90	265.	0.439131
120	425.	-0.1566
160	580.	0.

z km	u_0 m/s	u_0'' (m/s)/km^2
0	0.6	0.
10	-10.6	0.878224
15	0.3	-1.30935
20	-4.7	0.543157
30	-2.6	-0.2488
40	-7.4	0.0380408
50	-21.5	-0.461364
55	-30.6	2.2001
60	-9.7	-1.13904
65	-10.2	-2.77995
70	-49.8	2.87483
80	-16.7	-0.496515
95	21.8	-0.558837
110	-28.2	0.371864
125	-38.6	0.127382
140	-21.0	-0.134725
160	-22.6	0.

Table 1: Atmospheric sound speed and zonal wind data for the atmospheric model. v_i and v_i'' are values and second derivatives at z_i.

[3] Bogey, C., de Cacqueray, N., and Bailly, C. A shock-capturing methodology based on adaptative spatial filtering for high-order non-linear computations. *Journal of Computational Physics 228*, 5 (2009), 1447 – 1465.

[4] Dragna, D., Cotte, B., Blanc-Benon, P., and Poisson, F. Time-domain simulations of outdoor sound propagation with suitable impedance boundary conditions. *AIAA J. 49* (2011), 1420–1428.

[5] Gainville, O. *Modélisation de la propagation atmosphérique des ondes infrasonores par une méthode de tracé de rayons non linéaires*. PhD thesis, École centrale de Lyon, mai 2008. Num. 2008-07.

[6] Gainville, O., Blanc-Benon, P., Blanc, E., Roche, R., Millet, C., Piver, F. L., Despres, B., and Piserchia, P. F. *Misty Picture: A Unique Experiment for the Interpretation of the Infrasound Propagation from Large Explosive Sources*. Springer, 2009, pp. 575–598.

[7] Hanique-Cockenpot, G. *Etude numerique de la propagation non lineaire des infrasons dans l'atmosphere*. PhD thesis, Ecole Centrale Lyon, 2011.

[8] Korobeinikov. *Problems of Point-Blast Theory*. American Institute of Physics, 1985.

[9] Lutzky, M., and Lehto, D. L. Shock propagation in spherically symmetric exponential atmospheres. *Physics of Fluids 11*, 7 (1968), 1466–1472.

[10] Marsden, O. *Calcul direct du rayonnement acoustique de profils par une approche curviligne d'ordre eleve*. PhD thesis, Ecole Centrale Lyon, 2005.

[11] Marsden, O., Bogey, C., and Bailly, C. Direct noise computation of the turbulent flow around a zero-incidence airfoil. *AIAA J. 46* (2008), 874–883.

[12] Marsden, O., Vayno, L., Bogey, C., and Bailly, C. Study of long-range infrasound propagation with high-performance numerical schemes applied to the euler equations. In *13th Long Range Sound Propagation Symposium* (Lyon, France, 16-17 oct. 2008), pp. 201–216.

[13] Pierce, A. D. *Acoustics : An Introduction to Its Physical Principles and Applications*. Acoustical Society of America, 1994.

[14] Tam, C. K., and Dong, Z. Radiation and outflow boundary conditions for direct computation of acoustic and flow disturbances in a nonuniform mean flow. *Journal of Computational Acoustics 4*, 2 (1996), 175–201.